Ultrafine Cellulose Nanofiber-Assisted Physical and Chemical Cross-Linking of MXene Sheets for Electromagnetic Interference Shielding

Journal Article

Author(s):
Wu, Na; Zeng, Zhihui; Kummer, Nico; Han, Daxin; Zenobi, Renato; Nyström, Gustav

Publication date:
2021-12-15

Permanent link:
https://doi.org/10.3929/ethz-b-000511937

Originally published in:
Small Methods 5(12), https://doi.org/10.1002/smtd.202100889

Funding acknowledgement:
178765 - Soft ionization mass spectrometry for studying noncovalent interactions (SNF)

small methods
www.small-methods.com

Ultrafine Cellulose Nanofiber-Assisted Physical and Chemical Cross-Linking of MXene Sheets for Electromagnetic Interference Shielding

Na Wu, Zhihui Zeng, Nico Kummer, Daxin Han, Renato Zenobi,* and Gustav Nyström**

Transition metal carbides and nitrides (MXenes) have shown great potential for constructing thin, high-performance electromagnetic interference (EMI) shields. The challenges with these materials involve the weak interfacial interactions of MXenes, which results in inferior mechanical properties and structure of the MXene films and a conductivity/EMI shielding performance decay related to the poor MXene oxidation stability. Numerous efforts have been devoted to improving the mechanical properties or oxidation stability of the films, which always comes at the expense of EMI shielding performance. Here, ultrafine (≈1.4 nm) cellulose nanofibers are employed to achieve physical and chemical dual cross-linking of MXene (PC-MXene) nanosheets. The procedure involves drying of flexible and highly conductive PC-MXene films at ambient pressure and is energy-efficient and scalable. Compared to the MXene films, the PC-MXene films show significantly improved mechanical strength, hydrophobicity, oxidation stability, and are waterproof, without compromising the excellent EMI shielding effectiveness (SE). Moreover, the freestanding PC-MXene films reach a thickness of merely 0.9 µm and exhibit a high SE of 33.3 dB, which cannot be achieved by pure MXene films. This leads to ultrahigh thickness-specific SE and surface-specific SE values of 37 000 dB mm^{-1} and 148 000 dB cm^2 g^{-1} respectively, significantly surpassing those of previously reported MXene-based films.

1. Introduction

Electromagnetic interference (EMI) shielding materials are gaining importance because of the urgent need for electromagnetic compatibility of electronic devices and protection of biological tissue against harmful radiation.[1] High-performance EMI shields, involving high EMI shielding effectiveness (SE), low thickness and weight, good mechanical strength and flexibility, and considerable stability, are highly desirable.[2] Owing to the excellent electrical conductivity and the large aspect ratios, low-dimensional nanomaterials such as metal nanowires,[3] carbon nanotubes (CNTs),[4] graphene,[5] or transition metal carbides and nitrides (MXenes)[6] offer great potential for bottom–up construction of EMI shielding macrostructures. Among these materials, novel 2D MXene sheets, commonly known as $Ti_3C_2T_x$ MXenes, have attracted attention for constructing high-performance EMI shielding materials due to the metallic conductivity and the solution processability derived from their hydrophilic functional groups (−F, −O, and −OH).[7] For instance, vacuum filtrated MXene films showed an excellent EMI SE of 68 dB at a thickness of 11 µm.[8] This resulted in an ultrahigh surface-specific SE (SSE),[1b,8] defined as the SE divided by the thickness and density of shields, of 25 863 dB cm^2 g^{-1} for the MXene films. Compared to solid copper or stainless steel with SSE values of around 30 dB cm^2 g^{-1},[9] MXene-based films show great

N. Wu, R. Zenobi
Department of Chemistry and Applied Biosciences
ETH Zurich
8093 Zurich, Switzerland
E-mail: zenobi@org.chem.ethz.ch

Z. Zeng
School of Materials Science and Engineering
Shandong University
Jinan 250061, P. R. China
E-mail: zhihui.zeng@sdu.edu.cn

The ORCID identification number(s) for the author(s) of this article can be found under https://doi.org/10.1002/smtd.202100889.

DOI: 10.1002/smtd.202100889

Z. Zeng, N. Kummer, G. Nyström
Laboratory for Cellulose and Wood Materials
Swiss Federal Laboratories for Materials Science and Technology (Empa)
8600 Dübendorf, Switzerland
E-mail: gustav.nystroem@empa.ch

N. Kummer, G. Nyström
Department of Health Sciences and Technology
ETH Zürich
8092 Zürich, Switzerland

D. Han
Department of Information Technology and Electrical Engineering
ETH Zürich
8092 Zürich, Switzerland

potential for flexible, lightweight, and high-performance EMI shielding monoliths within next-generation electronics.

The main challenges for constructing thin, high-performance MXene-based shields include the weak interfacial interactions of MXenes, resulting in inferior mechanical performance of the corresponding macrostructures, and a loss of their EMI shielding performance due to poor oxidation stability.[10] The use of polymers as matrices or binders has been widely exploited to improve the mechanical strength or service stability of MXene-based shields.[11] For instance, MXene flakes have been dispersed in hydrophobic polymer matrices such as epoxy[12] or polyvinylidene fluoride,[13] to form composites with considerable mechanical strength and oxidation stability. By contrast, water-soluble polymers with abundant hydrophilic groups can form strong hydrogen bonding interactions with the MXenes,[14] avoiding severe agglomeration of MXene layers and thus achieving remarkably improved mechanical properties for the composites. Apart from the conductivity derived from the MXene conductive paths, the interfaces between MXene and polymers are vital for generating interfacial dipoles in the electric field of incident EM waves, promoting the EMI shielding performance. For example, vacuum-filtrated MXene films reinforced with sodium alginate,[8] aramid nanofiber,[15] and polyvinyl alcohol (PVA)[16] showed good EMI SE values of 57, 40, and 28 dB at thicknesses of 8, 3.2, and 100 μm, respectively, leading to ultrahigh SSE values ranging from 4770 to 50 491 dB cm^2 g^{-1}. However, water-soluble polymers fail to protect the MXene from oxidation due to their hydrophilicity, resulting in unsatisfactory MXene-based shields. Moreover, large insulating polymer gaps between the MXene nanosheets were introduced, inevitably deteriorating the electrical conductivity and EMI shielding performance of MXene/polymer composites. The intrinsically low mechanical strength of polymers also limited the preparation of ultrathin yet robust MXene-based monoliths. Although some inorganic nanomaterials[17] such as CNTs and graphene with good conductivity and mechanical strength could be integrated to improve the MXene-based shields, more complicated dispersion or recombination/composite processes for these inert nanomaterials were unavoidable thus inducing more efforts and costs. Last but not least, accomplishing an energy-efficient and scalable preparation method for high-performance MXene-based shields is vital for practical applications. Compared with the commonly used vacuum-assisted filtration[8,18] that requires low vacuum conditions and expensive substrates, ambient pressure drying of MXene-based freestanding shields is highly desirable yet rarely reported. For example, the blade-coated followed by ambient pressure-dried MXene films with excellent mechanical strength and EMI SE showed great potential for scalable production regardless of the hydrophilicity and low oxidation stability.[19] In short, facile and scalable manufacturing of robust and resilient MXene-based shields with high conductivity and EMI shielding performance remains challenging, especially to find a balance between these properties without substantially sacrificing one property over the other.

Cellulose nanofibers (CNFs),[20] made from the most abundant polymer on earth, can show diameters of a few to tens of nanometers, which is promising for minimizing the insulating gaps between conductive nanomaterials and thus a high electrical conductivity can be obtained.[21] With their good gelation capability, excellent mechanical strength, and large aspect ratios, CNFs can act as sustainable, biodegradable nanoscale binders of various nanomaterials, leading to an efficient construction of robust CNF-based EMI shields.[22] Although some CNF-reinforced MXene films prepared in the vacuum filtration approach showed considerable EMI SE at thicknesses of only tens of micrometers,[23] significantly compromised electrical conductivity and EMI shielding performance still existed. This can be ascribed to the relatively large diameters (above ten nanometers)[23a,b,e] of the CNFs employed, inevitably inducing large insulating gaps between the MXene layers. Here, we prepare 1D ultrafine (a diameter of merely 1.4 nm) and large-aspect-ratio (≈300) CNFs, aiming at maintaining the good conductivity and EMI SE of CNF-reinforced MXene-based films. Moreover, a strong chemical cross-linking of the MXene flakes is accomplished with the help of the CNFs in an ambient pressure drying approach. The ultrafine CNF-assisted physical and chemical dual cross-linking of MXene (PC-MXene) nanosheets contributes to the preparation of ultrathin, flexible, and highly conductive hybrid films, which show significantly improved mechanical strength, hydrophobicity, water resistance, and oxidation stability while maintaining the excellent EMI SE. Compared with the simple and commonly used silicone encapsulation treatment of MXene-based films to improve the hydrophobicity and oxidation stability,[24] more significant improvement in mechanical performance of our MXene-based films are obtained due to enhanced interfacial interactions between the building blocks. The thicknesses and CNF contents of the PC-MXene films are controlled effortlessly, allowing one to tune the EMI SE over a wide range. Furthermore, robust, freestanding PC-MXene with a thickness down to 0.9 μm still exhibited a satisfactory X-band EMI SE of 33.3 dB, which cannot be achieved by pure MXene films. Ultrahigh thickness-specific SE (SE/*d*, namely SE divided by the thickness) and SSE values of 37 000 dB mm^{-1} and 148 000 dB cm^2 g^{-1} are thus achieved respectively for our PC-MXene films significantly outperforming other freestanding MXene-based films. This work thus suggests a convenient, facile, low-cost, and scalable preparation approach for constructing high-performance MXene macrostructures with potential applications in next-generation flexible electronic devices and aerospace.

2. Results and Discussion

Figure 1a schematically illustrates the dual-cross-linking treatment of MXene-based films in an ambient pressure drying preparation process. An aqueous MXene dispersion with a high Zeta potential of around −40 mV was prepared by etching and delamination of a compact rock-like precursor Ti_3AlC_2 MAX (Figure S1, Supporting Information). The MXene flakes display an average lateral size of around 3 μm and a hexagonal atomic structure, as deduced from transmission electron microscopy (TEM) and electron diffraction data, respectively (Figure 1b). An atomic force microscope (AFM) image further shows a thickness (≈1.6 nm) of single-layer MXene (Figure 1c). In order to prepare ultrafine CNFs, we utilized 2,2,6,6-tetramethylpiperidin-1-oxyl (TEMPO)-mediated oxidation and grinding treatments to weaken the hydrogen bonds and strengthen the electrostatic repulsion between the cellulose chains from cellulose fibers. This leads to the scalable manufacturing of a stable CNF

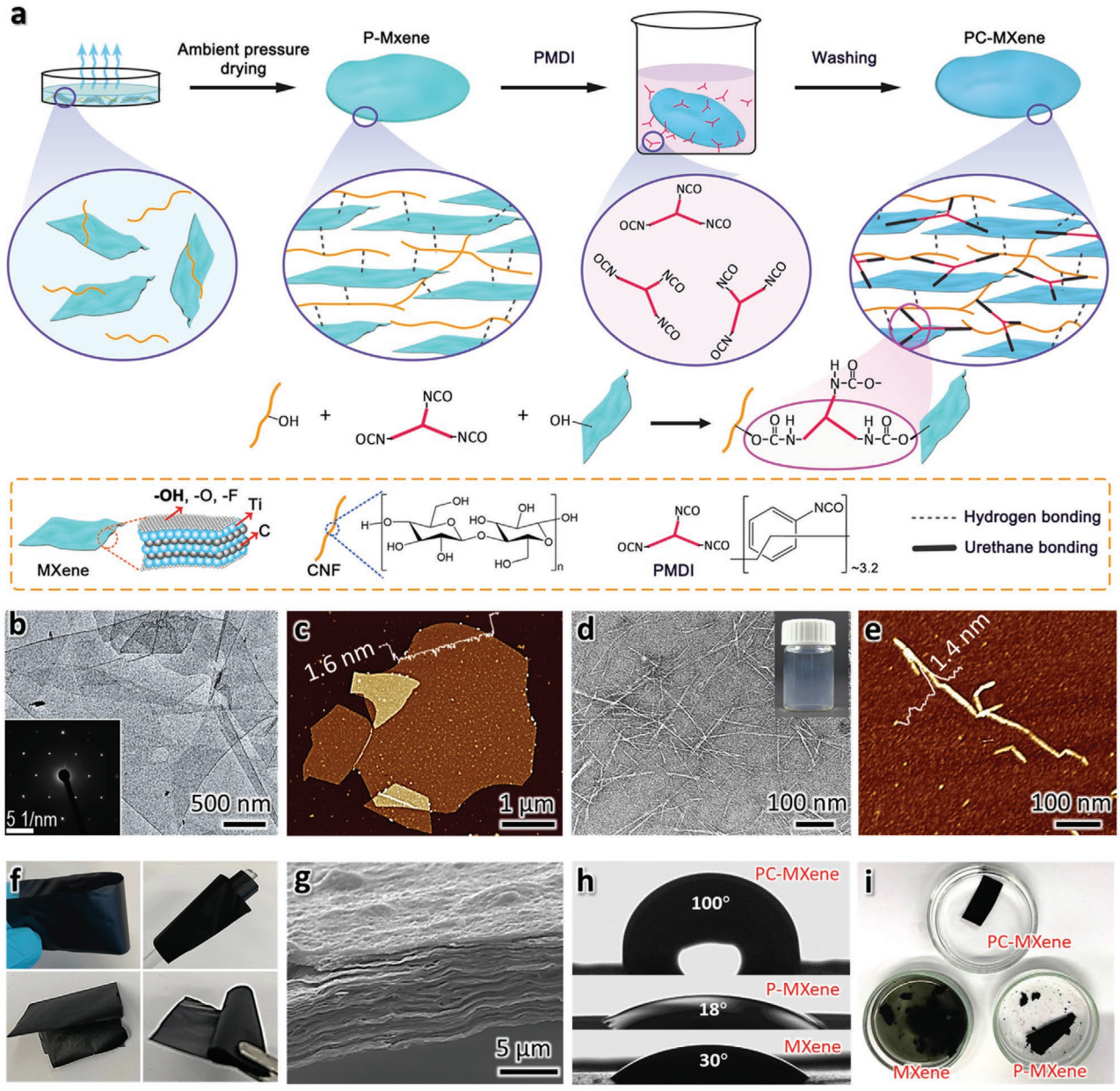

Figure 1. a) Schematic of the physical and chemical dual cross-linking preparation process for PC-MXene. b) TEM (inset shows electron diffraction image) and c) AFM (inset shows the height profile of a monolayer) images of the as-prepared MXene. d) TEM and e) AFM (inset shows the height of single fiber) of the as-prepared CNFs. f) Photographs and g) SEM images of the freestanding PC-MXene film (5 × 10 cm^2) showing ultraflexible performance including bendability, rollability, and foldability, at a thickness of 7.5 μm. h) Contact angles of the PC-MXene, P-MXene, and MXene films, i) Photograph of PC-MXene, P-MXene, and MXene films after ultrasonic treatment in water for 30 min, showing that the PC-MXene films are waterproof.

aqueous dispersion, showing a high Zeta potential of around −60 mV (Figure S2a,b, Supporting Information). TEM and AFM images show an average diameter of ≈1.4 nm and a large aspect ratio of ≈300 for 1D CNFs (Figure 1d,e). Similar hydrophilic functional groups of MXene and CNFs make for a stable MXene/CNF mixed dispersion with a high Zeta potential (Figure S2b,c, Supporting Information). Moreover, the CNFs adhered well to MXene due to strong hydrogen bonding interactions, leading to an intercalation between the MXene layers and the formation of a nacre-like "brick and mortar" microstructure[21b,23a] in physically cross-linked MXene (P-MXene) films (Figure 1a). This is instrumental for enhancing the mechanical strength of the P-MXene, which can be manufactured easily even at a low thickness of several micrometers. The ultrathin and robust P-MXene films were further chemically cross-linked, which not only further improved the mechanical strength, but also led to the change from hydrophilicity to hydrophobicity for the PC-MXene films. A typical, freestanding, and robust PC-MXene film with a size of 5 × 10 cm^2 and 30 wt% CNF exhibits excellent mechanical flexibility including bendability, rollability, and foldability (Figure 1f and Figure S3a, Supporting Information). The cross-sectional scanning electron microscope (SEM) image

of the PC-MXene films showed a layered structure and a thickness of around 7.5 µm (Figure 1g), which is similar to that of the P-MXene films (Figure S3b, Supporting Information). Compared with the similar mass of MXene films showing a density of 3.04 g cm^{-3} and a thickness of around 6 µm (Figure S3c,d, Supporting Information), the introduced CNFs[20a] result in a lower density of ≈2.5 g cm^{-3} and a higher thickness of ≈7.5 µm for the PC-MXene films. We also prepared the chemically cross-linked MXene (C-MXene) directly without adding CNFs. It is worth noting that the thickness of mechanically robust, free-standing PC-MXene films can be as low as 0.9 µm (as shown in the following part), which cannot be fulfilled by the pure MXene or C-MXene films. This is attributed to that reducing the thicknesses of mechanically brittle and weak MXene films without physical cross-linking was challenging in this ambient pressure drying method. In addition, dual cross-linking of MXene increases the water contact angles from 30° to 100° (Figure 1h), which is attributed to the introduction of the hydrophobic backbone in the chemical cross-linking agent poly((phenyl isocyanate)-*co*-formaldehyde) (PMDI). The wetting change as well as the strong noncovalent and covalent interactions between MXene and CNFs leads to excellent stability and water resistance (Figure 1g and Figure S4a, Supporting Information). After ultrasound treatment for 30 min of the MXene, P-MXene, and PC-MXene films immersed in water, MXene deteriorated completely, while the PC-MXene was quite stable. To summarize the material preparation, we utilized the effectiveness of physical and chemical dual cross-linking for ambient pressure dried preparation of ultrathin, flexible, robust, hydrophobic, and waterproof MXene-based macrostructures.

Fourier-transform infrared spectroscopy (FTIR) analysis confirmed the covalent cross-linking of the CNF, MXene, and

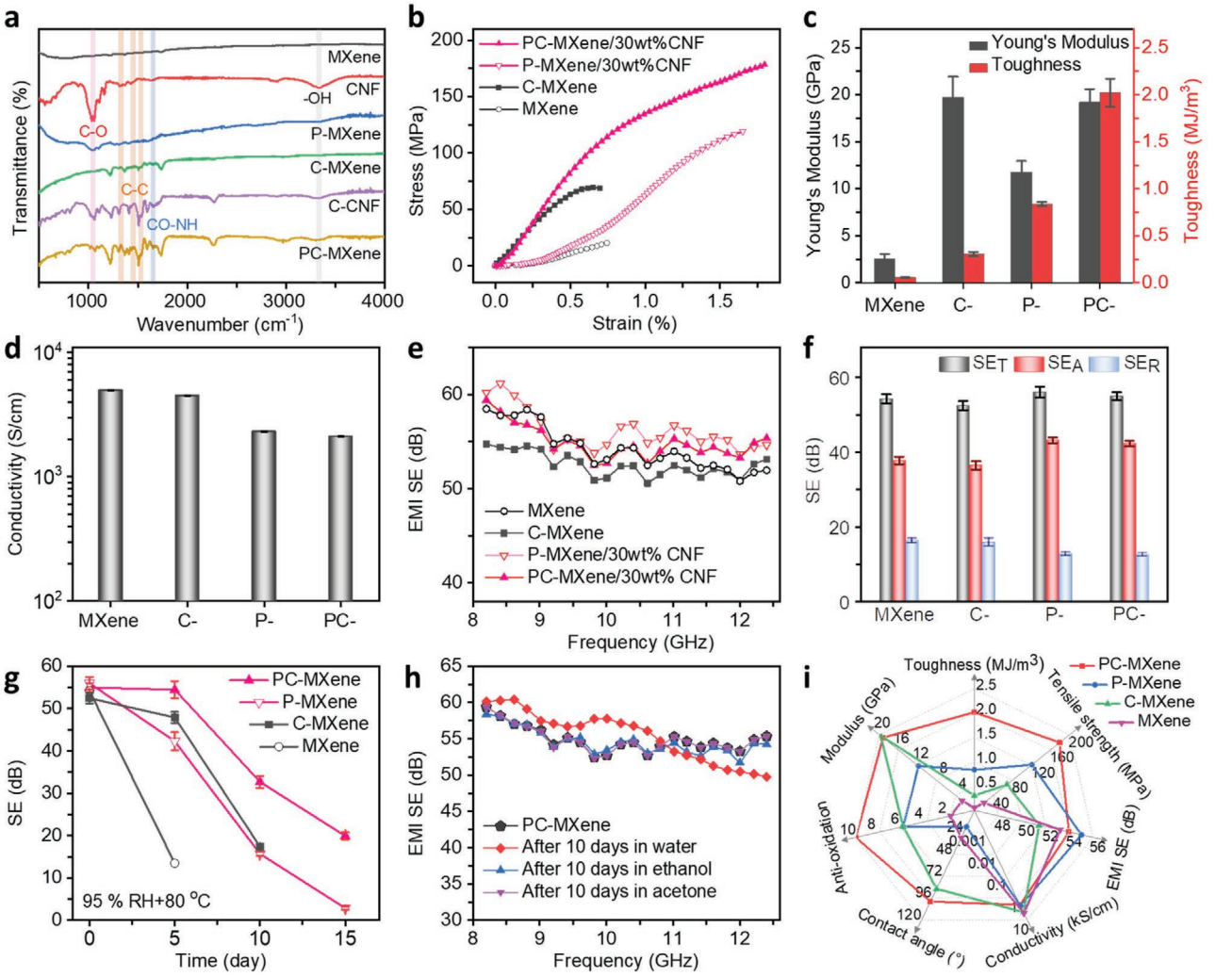

Figure 2. a) FTIR spectra of MXene- and CNF-based films, showing the physical and chemical cross-linking in PC-MXene. b) Tensile stress–strain curves of MXene, C-MXene, P-MXene (30 wt% CNF), and PC-MXene (30 wt% CNF) films and c) corresponding modulus and toughness. d) Electrical conductivity, e) X-band EMI SE, and f) EMI shielding performance (SE_T, SE_A, and SE_R) at 10 GHz of the MXene-based films with the similar mass. g) Change of SE as a function of time for the MXene, P-MXene (30 wt% CNF), and PC-MXene (30 wt% CNF) films stored in a 95% RH environment and a temperature of 70 °C. In the 1st day ($d = 0$), the films were in a dry state. h) EMI SE of MXene-based films after being immersed in various solvents. i) Radar plot of the properties of MXene-based films.

CNF/MXene composites caused by the incubation with PMDI (**Figure 2**a). A pure CNF film showed a characteristic C—O band at ≈1028 cm^{-1}. After chemical cross-linking, prominent bands at 1410, 1504, and 1596 cm^{-1} due to benzene ring skeletal modes of PMDI, and a peak at 1680 cm^{-1} corresponding to the amide I (CO—NH) mode derived from cross-linking of the —OH groups of CNF and —N=C=O groups of PMDI, appear.[25] The appearance of the characteristic bands of the benzene ring in the PMDI-incubated MXene films also verifies that PMDI has reacted with the hydroxyls of MXene. As expected, the FTIR spectrum of MXene/CNF (P-MXene) films shows the appearance of a C—O band (≈1028 cm^{-1}) derived from CNF. The new appearance of characteristic benzene ring vibrations and the CO—NH mode (1680 cm^{-1}) in PC-MXene verifies the successful chemical cross-linking of the P-MXene by PMDI. Furthermore, we also performed mass spectrometry to show the chemical cross-linking of PC-MXene films (Figure S5, Supporting Information). The introduction of covalent interactions between the MXenes and CNFs derived from the chemical cross-linker further led to the relatively higher thermal stability of the PC-MXene films than the P-MXene films (Figure S6a, Supporting Information). Moreover, XPS is also employed to show the efficient chemical cross-linking process of the MXene/CNF composite films (Figure S6b–d, Supporting Information). In short, PMDI could react with both MXene and CNF, forming a cross-linked network.

Either the physical or the chemical cross-linking of MXene leads to significantly enhanced mechanical properties, for example, the P-MXene films with 30 wt% CNF show larger tensile strength and fracture strain and the C-MXene films have a higher Young's modulus (Figure 2b,c) than the pure MXene films. The integration of both physical and chemical cross-links for the PC-MXene can lead to significant enhancement in tensile strength, modulus, and mechanical toughness, which show an increase of 786%, 646%, and 3383%, respectively, in comparison to those of MXene films. Moreover, the use of ultrafine CNFs will be beneficial to reduce the insulating gap between the conductive MXene layers in the composites, which can maintain the high electrical conductivities. The chemical cross-linking of MXene or MXene/CNF composite films does not significantly affect the electrical conductivity due to the formed conductive paths (Figure 2d). The conductivities of MXene, P-MXene, and PC-MXene films reach values of 4967, 2313, and 2113 S cm^{-1}, respectively, which show the same order of magnitude. Interestingly, the P-MXene and PC-MXene films reach slightly higher EMI SE values than pure MXene films at a similar mass, for example, average X-band SE values of the similar mass of MXene (≈5 μm), P-MXene (≈7.5 μm), and PC-MXene films (≈7.5 μm) reach 54.2, 56.0, and 55.0 dB, respectively (Figure 2e).

It is well known that the EMI shielding performance is dominated by reflection and absorption of incident electromagnetic waves,[1a,26] which depends on the presence of mobile charge carriers and electric (magnetic) dipoles, respectively. The total SE (SE_T) is the sum of shielding by reflection (SE_R) and absorption (SE_A). Moreover, interior interfaces/surfaces in the shielding architectures can lead to multiple reflections of incident waves and hence enhance the SE_A.[1b,4] In addition to the MXene terminal functional groups giving rise to electric dipoles under the electric field of the EM wave,[27] a large conductivity mismatch in the interfaces between the CNF and MXene can lead to strong interfacial polarization[28] and the layered microstructure and numerous interior interfaces are instrumental for multiple reflections[29] of incident EM waves. These are beneficial for improving the microwave absorption capability for MXene/CNF composite films, and thus the SE_A is increased even at a reduced MXene amount for both P-MXene (30 wt% CNF) and PC-MXene (30 wt% CNF) films (Figure 2f and Figure S7, Supporting Information). Here, the SE_A is dominant in the EMI shielding performance, which is similar to that of other reported MXene-based shielding architectures.[8,23a,c] Combined with the maintained high electrical conductivity contributing to a slightly reduced SE_R for MXene/CNF composites with 30 wt% CNF, slightly higher SE_T values were achieved for P-MXene and PC-MXene films.

To ascertain the service reliability or oxidation stability, we further compared the EMI SE over time for the MXene-based shields stored in a harsh condition containing a 95% RH humidity and a temperature of 70 °C (Figure 2g and Figure S8, Supporting Information). Pure MXene films deteriorate seriously within only 5 days, for example, the EMI SE is significantly decreased from 54.2 to 13.5 dB, and the films turn white and become very brittle and weak such that they can be easily damaged. In contrast, the CNFs' physical cross-linking is beneficial for maintaining the stability of P-MXene films even though the EMI SE significantly drops over time. Regarding the hydrophobic and strong PC-MXene films integrating both physical and chemical cross-links, even after stored in the harsh conditions for 15 days, the structure is stable, and EMI SE is maintained at a good value of around 20 dB. Particularly, the EMI SE is almost unchanged for PC-MXene films stored in this condition for 5 days. This demonstrates the vital role that the dual cross-linking of MXene plays in the oxidation stability against H_2O/O_2. Briefly, the introduction of the hydrophobic backbone in the chemical cross-linking agent PMDI contributes to the improved hydrophobicity of PC-MXene films, decreasing the contact of PC-MXene with the H_2O. Additionally, on the basis of the comparison between C-MXene and PC-MXene films, the formed strong chemical bonds derived from the reactions of PMDI with the hydrophilic functional groups in CNFs and MXene contribute to the mechanical and structural stability, which is beneficial for the oxidation stability of PC-MXene films in H_2O/O_2 condition. The significantly increased oxygen content of the P-MXene compared to PC-MXene after being stored in conditions with a 95% RH humidity and a temperature of 70 °C for 8 days further implies the improved oxidation stability of the PC-MXene films (Figure S9, Supporting Information). The strong cross-linking is also responsible for the stability of PC-MXene films against various solvents such as water, ethanol, and acetone, which can maintain similar EMI SE values even after being immersed in these solvents for 10 days at room temperature (Figure 2h and Figure S10, Supporting Information). The EMI SE also changes slightly for the PC-MXene films even after the 1000 times bending treatment, showing the stability upon mechanical deformation (Figure S11, Supporting Information). Therefore, as compared in the radar plots for MXene, C-MXene, P-MXene, and PC-MXene films (Figure 2i), we can easily ascertain that the dual cross-linking of MXene in the ambient pressure preparation approach is highly promising for manufacturing ultrathin, flexible, robust, highly

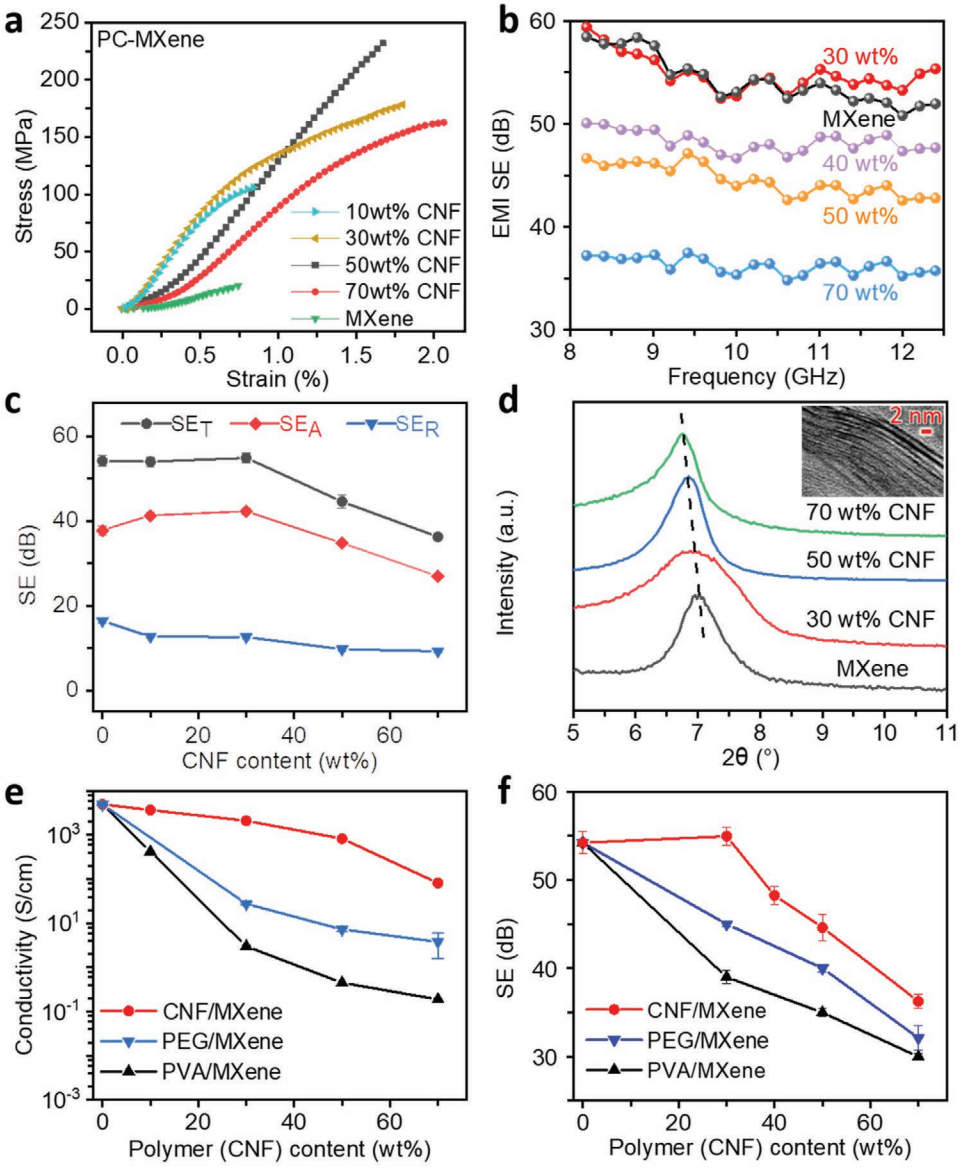

Figure 3. a) Tensile stress–strain curves of the PC-MXene films with various CNF contents. b) X-band EMI SE and c) EMI shielding performance (SE_T, SE_A, and SE_R) at 10 GHz of the similar mass of PC-MXene films with various CNF contents. d) XRD patterns of the PC-MXene films with various CNF contents (inset shows the TEM image of PC-MXene containing 30 wt% CNF, showing the MXene layers' interlayer gaps). e) Electrical conductivity and f) EMI SE for the similar mass of PC-MXene (CNF/MXene), PVA/MXene, and PEG/MXene composite films with various polymer contents.

reliable, and high EMI shielding performance MXene-based macrostructures.

In order to further understand the mechanism and the importance of the CNFs on the EMI shielding performance, we manufactured PC-MXene films with various CNF contents. Compared to pure MXene films, the tensile strength and modulus are significantly enhanced with introduced CNFs for the PC-MXene (**Figure 3**a). Nevertheless, excess CNFs lead to decreased mechanical strength and modulus because of decreased MXene and CNF-MXene interfaces, which are beneficial for the stress transfer[1b] in the composites. The PC-MXene films with 30–50 wt% CNFs show the highest mechanical strength and modulus. For the PC-MXene films, a CNF content of 30 wt% promotes a slightly increased SE_A and SE_T as discussed before. With further increasing CNF contents for PC-MXene films, significantly decreased MXene-CNF interfaces and charge carriers derived from MXene lead to a decrease of dominant SE_A and thus SE_T. However, high EMI SE values of PC-MXene films are maintained even with significantly increased CNF contents (Figure 3b,c), for example, the EMI SE still reaches 44.6 and 36.3 dB for the similar mass of PC-MXene films containing 50 and 70 wt% CNFs, respectively. These EMI SE values are much higher than a commercial SE value of 20 dB, which corresponds to a 99% attenuation of incident EM waves.[26b] In order to investigate the materials in more detail, we obtained the X-ray diffraction patterns of the PC-MXene films with various CNF contents to show the microstructure (Figure 3d). Owing to the intercalation of ultrafine CNFs, a

slight downshift of the (002) characteristic peak of the MXene-based films with increasing CNF content is observed. This corresponds to a slightly broadened interlayer spacing between MXene layers for PC-MXene films, for example, compared with that of 1.26 nm for pure MXene films, the PC-MXene films with 30 and 70 wt% CNFs show interlayer gaps of 1.28 and 1.31 nm, respectively. This agrees well with the MXenes' interlayer gap observed from the TEM image of PC-MXene containing 30 wt% CNF (inset of Figure 3d). This ultrathin insulating gap is beneficial for maintaining the high conductivity of the MXene/CNF hybrids. In comparison, we employed commonly used polymers such as PVA or polyethylene glycol (PEG) to prepare the MXene-based films with various polymer contents, and they show a more significant decrease in conductivities with increasing polymer contents (Figure 3e). For instance, MXene/PVA and MXene/PEG show conductivities of 0.45 and 7.3 S cm^{-1} respectively at polymer content of 50 wt%, which are two and three orders of magnitude lower than that of PC-MXene with 50 wt% CNF. The EMI SE values of these MXene-based films with the similar mass are also compared (Figure 3f). Herein, PC-MXene films show higher EMI SE than MXene/PVA and MXene/PEG at similar polymer mass ratios. For example, the X-band EMI SE values of PC-MXene, MXene/PVA, and MXene/PEG films reach around 45, 35, and 40 dB, respectively, and more importantly, the latter two cannot have higher EMI SE values at low polymer contents than pure MXene films. As reported,[23a,e] garlic husk and bacterial cellulose derivate CNFs, showing diameters of 20–50 and 20 nm, respectively, were applied to reinforce vacuum-filtrated MXene films, respectively. They showed EMI SE of 25.8 and 53.7 dB at thicknesses of 47 and 40 μm, respectively, which cannot perform as good as our PC-MXene films reinforced with ultrafine CNF. In short, our ultrafine CNFs efficiently demonstrate the superiority for manufacturing stronger MXene-based macrostructures without compromising the EMI SE.

In the ambient pressure drying approach, the PC-MXene films' thicknesses were effortlessly adjusted, leading to a wide-range controllability of EMI SE (**Figure 4**a–c). The EMI SE increases with increasing thicknesses, for example, the EMI SE reaches up to 73.8 dB at a thickness of 15 μm. More interestingly, owing to the robustness of the freestanding PC-MXene films, a thickness down to 0.9 μm was accomplished (Figure 4c and Figure S12, Supporting Information), which was a challenge for brittle and weak MXene only films. The EMI SE of PC-MXene still reaches high values of 33.3 dB at such a low thickness, which appears among the lowest values for that of previously reported freestanding shielding architectures satisfying the commercial SE value. Generally, achieving a higher SE associated with a minimum thickness is challenging for high-performance EMI shields.[7b,8] Therefore, the SE/d value as a critical index is used to evaluate the EMI shielding performance, and it can reach from 4920 to 37 000 dB mm^{-1} for the PC-MXene films significantly outperforming other shielding materials (Table S1, Supporting Information). The excellent performance is ascribed to the nacre-like "brick and mortar," layered structure of MXene nanosheets (Figure 4b,c) and introduced abundant and ultrathin interfaces between the MXene and CNFs, which synergistically contributed to excellent mechanical strength, remarkable electrical conductivity, strong interfacial polarization, and multiple reflections of incident EM waves (Figure 4d). In other words, the efficient design of ultrafine 1D CNFs and the strong dual cross-linking of MXene nanosheets lead to the excellent mechanical strength of PC-MXene without compromising the excellent EMI SE of MXene. In terms of tensile strength and EMI SE values, the PC-MXene films perform much better than other typical shielding macrostructures (Figure 4e). Further considering the low density, freestanding PC-MXene films show an SSE value up to 148 000 dB cm^2 g^{-1}, outperforming that of the other MXene-based films ever reported (Figure 4f). More detailed information for the comparisons of typical EMI shielding materials is concluded in Table S1, Supporting Information, for example, even at a high EMI SE of more than 70 dB, the PC-MXene films have an SSE value of 19 680 dB cm^2 g^{-1}, which is two–three orders higher than that of most commonly used polymer nanocomposites owning SSE values ranging from tens to hundreds. Combined with the hydrophobicity and service stability, as well as the facile preparation method, the ultrathin, flexible, and robust PC-MXene films with outstanding EMI shielding performance offer great promises in the application areas of aircraft, spacecraft, portable electronics, and smart wearable devices.

3. Conclusions

We employed sustainable CNFs to assist in physical and chemical dual cross-linking of MXene nanosheets in a facile ambient pressure drying preparation approach. Ultrafine, robust, and large-aspect-ratio CNFs and dual cross-linking lead to the significantly improved mechanical properties, good hydrophobicity as well as excellent water and oxidation stability for the PC-MXene films without compromising the outstanding EMI SE of the MXene flakes. Compared with other MXene-based polymer nanocomposites, our CNF/MXene composites perform much better in electrical conductivity and EMI SE at similar polymer contents. This is ascribed to the synergistic interactions of the ultrafine CNFs and MXene, enabling excellent conductivity, efficient interfacial polarization, and layered microstructure for the PC-MXene films. The flexible, freestanding PC-MXene films can reach EMI SE values of 33.3 to 73.8 dB at thicknesses of 0.9 to 15 μm, respectively. The SE/d and SSE values of the PC-MXene are up to 37 000 dB mm^{-1} and 148 000 dB cm^2 g^{-1}, respectively, significantly surpassing those of other MXene-based films ever reported. This work demonstrates a convenient, facile, low-cost, and scalable preparation approach for constructing high-performance MXene-based macrostructures having potential for the development of next-generation flexible and high-performance electronic devices and for applications in aerospace.

4. Experimental Section

Preparation of MXene Aqueous Dispersion: Aqueous dispersions of MXene were prepared by etching of the aluminum phase followed by the mechanical delamination process of the precursor Ti_3AlC_2 MAX. First, 3.2 g lithium fluoride (Sigma Aldrich, USA) was dissolved in 40 mL hydrochloric acid (9 M, Sigma Aldrich, USA) in a magnetic stirrer. Then, 2.0 g Ti_3AlC_2 MAX (Laizhou Kai Kai Ceramic Materials Co., Ltd., China) was added to that solution under stirring for 40 min, and the dispersion

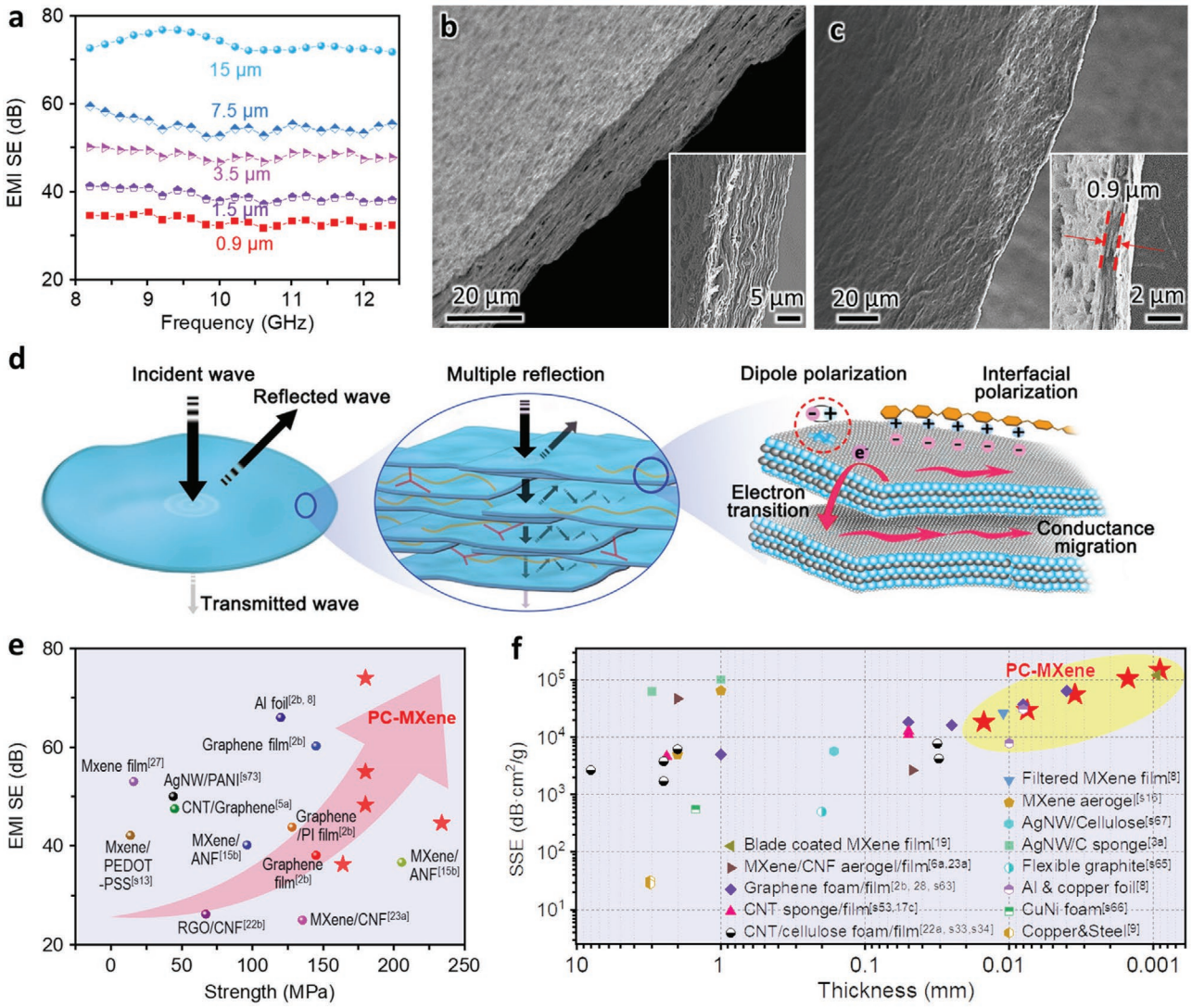

Figure 4. a) X-band EMI SE of PC-MXene films (30 wt% CNF) with various thicknesses, and SEM images of PC-MXene (30 wt% CNF) films showing thicknesses of b) 15 and c) 0.9 μm. d) Schematic showing the proposed EMI shielding mechanism of the PC-MXene films for ultrahigh EMI shielding performances. Comparison of the PC-MXene films' shielding performance with other shielding materials: e) EMI SE and tensile strength of typical EMI shielding films and f) SSE values of typical EMI shielding macrostructures with various thicknesses.

was heated to 35 °C for 24 h. The mixture was then washed several times by centrifuging at 3500 rpm and redispersing the pellet in ultrapure water until a pH of ≈6 was reached when the multilayered MXene started to delaminate. Finally, after the suspension was vigorously shaken for 20 min and centrifuged for 10 min at 3800 rpm, the supernatant MXene dispersion was recovered.

Preparation of Cellulose Nanofiber Aqueous Dispersion: In order to obtain ultrafine CNFs, elemental chlorine free fibers extracted from bleached softwood pulp fibers (Mercer Stendal Company, Berlin, Germany) were processed by a TEMPO oxidation and mechanical grinding process.[22c] First, TEMPO and sodium bromide (NaBr) were dissolved in water, obtaining concentrations of 0.1 and 1.0 mmol g^{-1} of cellulose pulp, respectively. The solution was mixed with a 2 wt% aqueous cellulose fiber suspension. The pH of the suspension was adjusted to around 10 by adding sodium hydroxide solution (1 mol L^{-1}), and 10 mmol sodium hypochlorite per gram of cellulose pulp was employed for the reaction. After the reaction, the authors' could obtain the TEMPO-oxidized cellulose fibers by washing until a constant conductivity to the distilled water was reached. Subsequently, the TEMPO oxidized cellulose fibers aqueous suspensions were ground by a Supermass Collider (MKZA10-20J CE Masuko Sangyo, Japan). The energy consumption of the process was recorded with a power meter, being 9 kWh kg^{-1} of dried cellulose pulp. After the treatment, the stable TEMPO-oxidized CNF aqueous dispersion was obtained.

Preparation of MXene/Cellulose Nanofiber Composite Films with Dual Cross-Linking: The MXene and CNF dispersions were adjusted to a similar concentration (≈0.5 wt%) and mixed by magnetic stirring for 1 h at various MXene/CNF ratios as precursor dispersion. Then, the precursor dispersions were dried at 50 °C in a polypropylene mold, forming the ambient pressure dried freestanding MXene/CNF (P-MXene) films containing various CNF mass ratios. The pure MXene films were also prepared from pure MXene dispersions in the same process. Afterward, the pure MXene and P-MXene films were chemically cross-linked by PMDI. Herein, PMDI was dissolved in acetonitrile/methyl caproate (4:1 v/v) solution at a volume ratio of 1:9, then the MXene and P-MXene films were immersed in this acetonitrile/methyl caproate (4:1 v/v) solution with a 10% PMDI. After reacting in the oven for 2 h at 70 °C, the films were washed with acetone and dried in the air. The remaining PMDI solution was recycled into a dry sealed bottle and could be reused. Finally, freestanding C-MXene and PC-MXene films with

various CNF contents were manufactured. The thicknesses of PC-MXene were adjusted by controlling the mass of the precursor dispersion.

Characterization: The morphology and structure of the CNF and MXene were characterized by TEM (JEOL JEM2200fS) and AFM (Bruker ICON3). SEM (FEI NanoSEM 230) was also performed, to characterize the microstructures of the MXene-based films. A drop shape analyzer (DSA 30, Krüss, Germany) was used to measure the water contact angles of the MXene-based films. An FTIR spectrometer (Perkin Elmer Spectrum Two) with an attenuated total reflection accessory was used to perform the FTIR measurements, confirming the cross-linking of MXene-based films. The cross-linking of the PC-MXene was also analyzed with the MALDI-TOF/TOF mass spectrometer (model 4800 plus, AB Sciex, Darmstadt, Germany), which was equipped with a high-mass detector (HM2, CovalX AG, Zurich, Switzerland). The MXene-based films were fixed onto the surface of a stainless steel plate with double faced adhesive copper tape; then the authors successively deposited 2,5-dihydroxybenzoic acid (50 mg mL^{-1}, dissolved in 1:500:500 v/v/v trifluoroacetic acid/water/acetonitrile) and 10 mg mL^{-1} NaI on the films. After drying the films in air, the samples were tested. Each mass spectrum was the average of 400 laser shots acquired at random sample positions. The tensile stress–strain curves of the MXene-based films were obtained by a dynamic mechanical analysis (TA Q800), and at least three samples for each component were tested. The resistances (R) of the MXene-based films were measured in a four-probe method by a Keithley 4200 electrometer at room temperature. The resistance values were further used to calculate the electrical conductivity (δ) by the equation $\delta = l/(R{\cdot}A)$, where A and l were the effective area and length, respectively. The waveguide method using a vector network analyzer (Agilent 8517A) was utilized to measure EMI SE in the frequency range of 8.2–12.4 GHz (X-band) of the films with size of 22.86 mm × 10.16 mm (length × width). More than three specimens were tested for each component. The S-parameters of each film were recorded and used to calculate the SE_T, SE_R, and SE_A.

Supporting Information

Supporting Information is available from the Wiley Online Library or from the author.

Acknowledgements

N.W. and Z.Z. contributed equally to this work. The authors thank Prof. Dr. Colombo Bolognesi from ETH Zürich and Anja Huch from Empa for providing suggestion and help for the characterization in the course of this work. Moreover, the authors acknowledge funding from the Swiss National Science Foundation (to R.Z., grant no. 200020_178765) and the support from the Chinese Scholarship Council (to N.W., project # 201709370040).

Open access funding provided by Eidgenossische Technische Hochschule Zurich.

Conflict of Interest

The authors declare no conflict of interest.

Data Availability Statement

Research data are not shared.

Keywords

cross-linking, electromagnetic interference shielding, lightweight, MXenes, nanocellulose

Received: August 3, 2021
Revised: September 24, 2021
Published online: October 20, 2021

[1] a) A. Iqbal, F. Shahzad, K. Hantanasirisakul, M.-K. Kim, J. Kwon, J. Hong, H. Kim, D. Kim, Y. Gogotsi, C. M. Koo, *Science* **2020**, *369*, 446; b) Z. Zeng, H. Jin, M. Chen, W. Li, L. Zhou, Z. Zhang, *Adv. Funct. Mater.* **2016**, *26*, 303; c) Y. Zhang, Y. Huang, T. Zhang, H. Chang, P. Xiao, H. Chen, Z. Huang, Y. Chen, *Adv. Mater.* **2015**, *27*, 2049.

[2] a) Z. Zeng, F. Jiang, Y. Yue, D. Han, L. Lin, S. Zhao, Y. B. Zhao, Z. Pan, C. Li, G. Nystrom, J. Wang, *Adv. Mater.* **2020**, *32*, e1908496; b) Q. Wei, S. Pei, X. Qian, H. Liu, Z. Liu, W. Zhang, T. Zhou, Z. Zhang, X. Zhang, H. M. Cheng, W. Ren, *Adv. Mater.* **2020**, *32*, 1907411.

[3] a) Y.-J. Wan, P.-L. Zhu, S.-H. Yu, R. Sun, C.-P. Wong, W.-H. Liao, *Small* **2018**, *14*, 1800534; b) S. Wu, M. Zou, Z. Li, D. Chen, H. Zhang, Y. Yuan, Y. Pei, A. Cao, *Small* **2018**, *14*, 1800634.

[4] Z. Zeng, H. Jin, M. Chen, W. Li, L. Zhou, X. Xue, Z. Zhang, *Small* **2017**, *13*, 1701388.

[5] a) Q. Song, F. Ye, X. Yin, W. Li, H. Li, Y. Liu, K. Li, K. Xie, X. Li, Q. Fu, L. Cheng, L. Zhang, B. Wei, *Adv. Mater.* **2017**, *29*, 1701583; b) B. Wen, M. Cao, M. Lu, W. Cao, H. Shi, J. Liu, X. Wang, H. Jin, X. Fang, W. Wang, J. Yuan, *Adv. Mater.* **2014**, *26*, 3484.

[6] a) Z. Zeng, C. Wang, G. Siqueira, D. Han, A. Huch, S. Abdolhosseinzadeh, J. Heier, F. Nuesch, C. J. Zhang, G. Nystrom, *Adv. Sci.* **2020**, *7*, 2000979; b) W. Chen, L. X. Liu, H. B. Zhang, Z. Z. Yu, *ACS Nano* **2020**, *14*, 16643; c) Z. Zeng, E. Mavrona, D. Sacré, N. Kummer, J. Cao, L. A. E. Müller, E. Hack, P. Zolliker, G. Nyström, *ACS Nano* **2021**, *15*, 7451; d) S. Shi, B. Qian, X. Wu, H. Sun, H. Wang, H.-B. Zhang, Z.-Z. Yu, T. P. Russell, *Angew. Chem., Int. Ed.* **2019**, *58*, 18171.

[7] a) D. Nepal, W. J. Kennedy, R. Pachter, R. A. Vaia, *ACS Nano* **2021**, *15*, 21; b) T. Yun, H. Kim, A. Iqbal, Y. S. Cho, G. S. Lee, M. K. Kim, S. J. Kim, D. Kim, Y. Gogotsi, S. O. Kim, C. M. Koo, *Adv. Mater.* **2020**, *32*, 1906769; c) M. Han, C. E. Shuck, R. Rakhmanov, D. Parchment, B. Anasori, C. M. Koo, G. Friedman, Y. Gogotsi, *ACS Nano* **2020**, *14*, 5008.

[8] F. Shahzad, M. Alhabeb, C. B. Hatter, B. Anasori, S. M. Hong, C. M. Koo, Y. Gogotsi, *Science* **2016**, *353*, 1137.

[9] X. Shui, D. D. L. Chung, *J. Electron. Mater.* **1997**, *26*, 928.

[10] a) H. Chen, Y. Wen, Y. Qi, Q. Zhao, L. Qu, C. Li, *Adv. Funct. Mater.* **2019**, *30*, 1906996; b) Y.-J. Wan, K. Rajavel, X.-M. Li, X.-Y. Wang, S.-Y. Liao, Z.-Q. Lin, P.-L. Zhu, R. Sun, C.-P. Wong, *Chem. Eng. J.* **2021**, *408*, 127303; c) X. Zhao, A. Vashisth, E. Prehn, W. Sun, S. A. Shah, T. Habib, Y. Chen, Z. Tan, J. L. Lutkenhaus, M. Radovic, M. J. Green, *Matter* **2019**, *1*, 513.

[11] a) P. Song, B. Liu, H. Qiu, X. Shi, D. Cao, J. Gu, *Compos. Commun.* **2021**, *24*, 100653; b) M. Carey, M. W. Barsoum, *Mater. Today Adv.* **2021**, *9*, 100120.

[12] L. Wang, L. Chen, P. Song, C. Liang, Y. Lu, H. Qiu, Y. Zhang, J. Kong, J. Gu, *Composites, Part B* **2019**, *171*, 111.

[13] K. Rajavel, S. Luo, Y. Wan, X. Yu, Y. Hu, P. Zhu, R. Sun, C. Wong, *Composites, Part A* **2020**, *129*, 105693.

[14] a) X. Jin, J. Wang, L. Dai, X. Liu, L. Li, Y. Yang, Y. Cao, W. Wang, H. Wu, S. Guo, *Chem. Eng. J.* **2020**, *380*, 122475; b) Z. Zhou, J. Liu, X. Zhang, D. Tian, Z. Zhan, C. Lu, *Adv. Mater. Interfaces* **2019**, *6*, 1802040; c) Z. Ling, C. E. Ren, M.-Q. Zhao, J. Yang, J. M. Giammarco, J. Qiu, M. W. Barsoum, Y. Gogotsi, *Proc. Natl. Acad. Sci. USA* **2014**, *111*, 16676.

[15] a) F. Xie, F. Jia, L. Zhuo, Z. Lu, L. Si, J. Huang, M. Zhang, Q. Ma, *Nanoscale* **2019**, *11*, 23382; b) C. Weng, T. Xing, H. Jin, G. Wang, Z. Dai, Y. Pei, L. Liu, Z. Zhang, *Composites, Part A* **2020**, *135*, 105927.

[16] H. Xu, X. Yin, X. Li, M. Li, S. Liang, L. Zhang, L. Cheng, *ACS Appl. Mater. Interfaces* **2019**, *11*, 10198.

[17] a) S. Zhao, H.-B. Zhang, J.-Q. Luo, Q.-W. Wang, B. Xu, S. Hong, Z.-Z. Yu, *ACS Nano* **2018**, *12*, 11193; b) L. Wang, H. Qiu, P. Song, Y. Zhang, Y. Lu, C. Liang, J. Kong, L. Chen, J. Gu, *Composites, Part A*

2019, *123*, 293; c) R. Yang, X. Gui, L. Yao, Q. Hu, L. Yang, H. Zhang, Y. Yao, H. Mei, Z. Tang, *Nano-Micro Lett.* **2021**, *13*, 66.
[18] C. Ma, W.-T. Cao, W. Zhang, M.-G. Ma, W.-M. Sun, J. Zhang, F. Chen, *Chem. Eng. J.* **2021**, *403*, 126438.
[19] J. Zhang, N. Kong, S. Uzun, A. Levitt, S. Seyedin, P. A. Lynch, S. Qin, M. Han, W. Yang, J. Liu, X. Wang, Y. Gogotsi, J. M. Razal, *Adv. Mater.* **2020**, *32*, 2001093.
[20] a) T. Li, C. Chen, A. H. Brozena, J. Y. Zhu, L. Xu, C. Driemeier, J. Dai, O. J. Rojas, A. Isogai, L. Wågberg, L. Hu, *Nature* **2021**, *590*, 47; b) B. Thomas, M. C. Raj, A. K. B., R. M. H., J. Joy, A. Moores, G. L. Drisko, C. Sanchez, *Chem. Rev.* **2018**, *118*, 11575.
[21] a) K. De France, Z. Zeng, T. Wu, G. Nyström, *Adv. Mater.* **2021**, *33*, 2000657; b) W. Tian, A. VahidMohammadi, M. S. Reid, Z. Wang, L. Ouyang, J. Erlandsson, T. Pettersson, L. Wågberg, M. Beidaghi, M. M. Hamedi, *Adv. Mater.* **2019**, *31*, 1902977.
[22] a) Z. Zeng, C. Wang, T. Wu, D. Han, M. Luković, F. Pan, G. Siqueira, G. Nyström, *J. Mater. Chem. A* **2020**, *8*, 17969; b) W. Yang, Z. Zhao, K. Wu, R. Huang, T. Liu, H. Jiang, F. Chen, Q. Fu, *J. Mater. Chem. C* **2017**, *5*, 3748; c) Z. Zeng, T. Wu, D. Han, Q. Ren, G. Siqueira, G. Nystrom, *ACS Nano* **2020**, *14*, 2927.
[23] a) W.-T. Cao, F.-F. Chen, Y.-J. Zhu, Y.-G. Zhang, Y.-Y. Jiang, M.-G. Ma, F. Chen, *ACS Nano* **2018**, *12*, 4583; b) Z. Zhan, Q. Song, Z. Zhou, C. Lu, *J. Mater. Chem. C* **2019**, *7*, 9820; c) W. Cao, C. Ma, S. Tan, M. Ma, P. Wan, F. Chen, *Nano-Micro Lett.* **2019**, *11*, 72; d) Q. Liu, Y. Zhang, Y. Liu, Z. Liu, B. Zhang, Q. Zhang, *J. Alloys Compd.* **2021**, *860*, 158151; e) Z. Cui, C. Gao, Z. Fan, J. Wang, Z. Cheng, Z. Xie, Y. Liu, Y. Wang, *J. Electron. Mater.* **2021**, *50*, 2101.
[24] a) Q.-W. Wang, H.-B. Zhang, J. Liu, S. Zhao, X. Xie, L. Liu, R. Yang, N. Koratkar, Z.-Z. Yu, *Adv. Funct. Mater.* **2019**, *29*, 1806819; b) C. Ma, Q. Yuan, H. Du, M. G. Ma, C. Si, P. Wan, *ACS Appl. Mater. Interfaces* **2020**, *12*, 34226; c) Z. Zhou, Q. Song, B. Huang, S. Feng, C. Lu, *ACS Nano* **2021**, *15*, 12405.
[25] T. Wu, Z. Zeng, G. Siqueira, K. De France, D. Sivaraman, C. Schreiner, R. Figi, Q. Zhang, G. Nyström, *Nanoscale* **2020**, *12*, 7383.
[26] a) D. D. L. Chung, *Carbon* **2001**, *39*, 279; b) J.-M. Thomassin, C. Jérôme, T. Pardoen, C. Bailly, I. Huynen, C. Detrembleur, *Mater. Sci. Eng., R* **2013**, *74*, 211.
[27] J. Liu, H.-B. Zhang, R. Sun, Y. Liu, Z. Liu, A. Zhou, Z.-Z. Yu, *Adv. Mater.* **2017**, *29*, 1702367.
[28] N. Yousefi, X. Sun, X. Lin, X. Shen, J. Jia, B. Zhang, B. Tang, M. Chan, J. K. Kim, *Adv. Mater.* **2014**, *26*, 5480.
[29] Z. Chen, C. Xu, C. Ma, W. Ren, H. M. Cheng, *Adv. Mater.* **2013**, *25*, 1296.